X-Ray Tomography of CP Titanium Friction Stir Welds Incorporating Fiducial Markers

R. K. Everett*, A. C. Lewis*, J. Wolk‡, C. Scheck‡, S. Szpara‡, S. Nimer†, M. Zupan†

*Naval Research Laboratory
Washington, DC 20375

‡ Naval Surface Warfare Center - Carderock Division
Bethesda, MD 20817

†University of Maryland Baltimore County
Baltimore, MD 21250

Keywords: x-ray, tomography, friction stir welding, titanium

Abstract – Friction stir welding (FSW) of titanium has the potential to reduce fabrication and life-cycle costs, as well as joint and process complexity compared to conventional joining techniques. However, commercial-purity (CP) Ti has been found to be rather difficult to FS weld. Voids are frequently present, and control over weld consistency and quality is challenging. In this paper, we report on the use of markers, placed in FS welds, to aid flow visualization, process comprehension, and parameter optimization. Nickel (Ni) foil markers were incorporated in 6 mm (0.25 inch) thick CP titanium friction stir welds of various geometries using simple frustum-shaped tools. X-ray computed microtomography (XCMT), EDS and EBSD, as well as standard optical- and electron- microscopy techniques, have been utilized to study marker location and distribution, and material microstuctures in these welds. The presence of the Ni markers affects welding loads, surface finish, and the presence of voids compared to standard processing. The markers clearly show differences in material deposited in the advancing and retreating sides, and are capable of delineating different flows at different depths. Direct local material property measurements using microtensile samples (nominally 3mm long and 1mm wide) from the weld and transitions zones measures mechanical properties comparable to the base metal.

I. Introduction – Titanium (Ti) alloys can provide weight reduction and reduced total operational costs because of high corrosion/erosion resistance. However, high fabrication costs may limit many titanium applications. Titanium alloys have been joined through conventional fusion welding techniques such as gas tungsten arc welding (GTAW) and gas metal arc welding (GMAW). Friction stir welding (FSW) of titanium has the potential to reduce fabrication and life-cycle costs, as well as joint and process complexity compared to conventional joining techniques because it does not require the use of filler material and has the potential for up to ½" depth of penetration in a single pass with high weld soundness. Additionally, joining below melting temperature may reduce contamination. A highly automated process, FSW also has the potential to reduce inspection requirements.

Early investigations showed promise for friction stir welding of some titanium alloys [1, 2]. However, commercial-purity (CP) Ti has been found to be rather difficult to FS weld. Voids are frequently present, and control over weld consistency and quality is difficult.

Markers have been placed in FS welds to aid flow visualization, and process comprehension and optimization. Markers are materials, usually, spheres, wires or foils of some contrasting element, that are placed in the joint to be welded. When the marked joints are processed, the distribution of marker material indicates the final resting position and hopefully denotes

the movement of the parent metal. Two recent examples of using fiducial markers to study the FSW process are the work of Lorrain et al. [3] and Mukherjee and Ghosh [4].

X-ray computed microtomography (XCMT) has been utilized to study voids in metals [5, 6], and in FS welds in titanium [7]. Copper foil markers [8] and lead wires [9] have been used in aluminum FS welds to create contrast in tomograms. In this paper, we report on the initial use of nickel foil markers in CP titanium friction stir welds. The paper is organized as follows: Section 2 will cover sample preparation and initial optical characterization; Section 3 will cover the x-ray tomography and results; Section 4 will review further characterization performed to record and understand the observed microstructure; Section 5 will present some preliminary mechanical properties, and Section 6 will summarize and discuss future directions.

II. Sample Preparation

Plates of CP Ti, 305 x 152 x 6 mm thick, were prepared for FS welding by mild abrasion and degreasing. A 6.35 x 0.1 mm commercially pure, annealed Ni foil strip was placed in the butt joint interface and held in place by clamping. Half of the length of the joint was prepared with the foil present, and half without, such that the joint without Ni foil was welded first. Other tests, not reported here, have been conducted with thicker 12 mm plates, thinner 0.05 mm Ni foils, and with the foil along the whole length of the joint.

FSW

FS welding was performed on an MT S ISTIR PDS system using a 10% lanthanated tungsten tool with a tapered probe and narrow shoulder. The shoulder diameter is 22.86 mm (0.9 inch). The inserted region is 7.92 mm (0.312 inch) in diameter tapering at 20 degrees to a depth of 6.35 mm (0.25 inch) where the final diameter is 4.75 mm (0.187 inch). This was inserted in to a holder made of Densimet. FS welding was conducted with a tool rotation speed of 300 rpm, and a tool travel speed of 25.4 mm/min. These conditions translate into an 85 μm advance per revolution. Tool rotations as high as 500 rpm and translation speeds as fast as 101.6 mm/min (4 ipm) have been investigated but are not discussed here.

After welding, samples were sectioned from both no foil and foil areas of the plate for metallographic and tomographic analysis. Figure 1 presents typical examples from each region. Note the smoother surface finish of the sample incorporating the nickel foil.

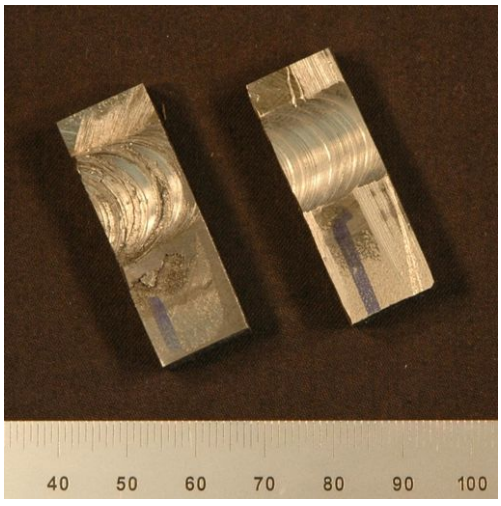

Figure 1 – Photograph of the top surfaces of friction stir welded CP Ti with no foil (left) and Ni foil present (right) in the interface.

Metallography

Samples were prepared for metallurgical analysis by conventional polishing techniques. A final “super” Kroll’s etch was given to highlight the macrostructure of the welds. Figures 2a and 2b are low magnification optical micrographs showing the structure of the FS weld with no foil (Fig. 2a) and with Ni foil present (Fig. 2b). The CP Ti FS weld in Figure 2a clearly has large voids present, whereas no voids have been seen in the Ni foil weld. Both macrostructures reflect the basic shape of the tool, but the Ni foil weld exhibits a larger process zone. High magnification images of the deformed Ni foil remaining at the bottom of the plate along the original joint line show no indications of intermetallic formation. Horizontal and vertical Vickers microhardness traverses were performed on the polished samples. Values are similar (Hv=194 with Ni foil versus Hv=182 without) and are consistent with previous reported work [10]. Except for one anomalous measurement (perhaps taken on tool debris), the two samples measure remarkably similar.

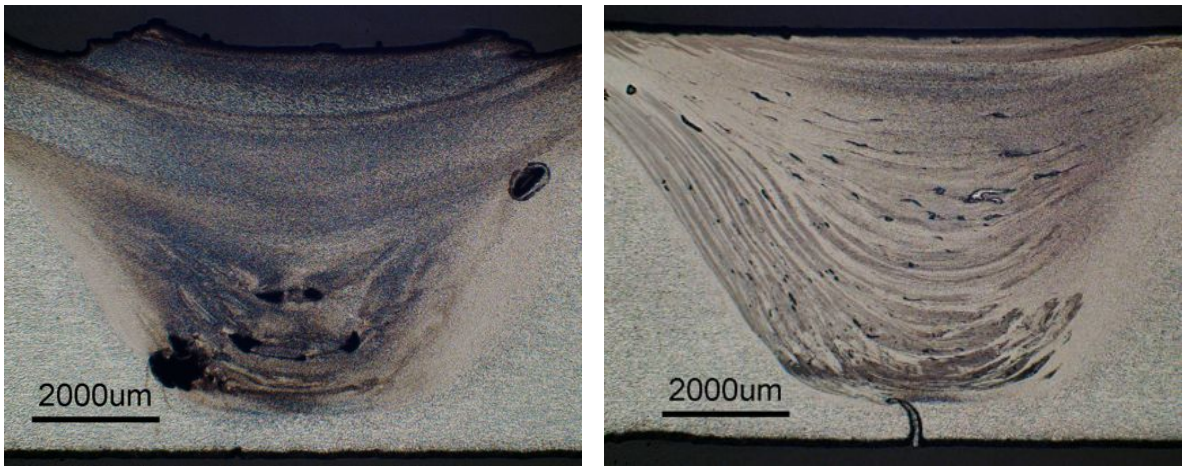

(a) **(b)**

Figure 2 – Photographs of (a) CP Ti FS weld without marker foil and (b) with Ni marker foil. Weld direction is out of the page.

III - XCMT

A low speed diamond saw with an oil-based lubricant was used to slice specimens approximately 6 x 40 x 2.8 mm thick from the welded plate. All x-ray tomograms presented here were taken using a Skyscan model 1172 tomography system with a 1.3 Megapixel camera. Scans were performed using a 100 kV x-ray source voltage setting with an image voxel size of 14.8 microns and 0.45 degree rotation steps (400 images). Single scans took about 40 minutes. Image cone-beam reconstruction was performed using the Skyscan proprietary software (NRECON) [11]. Ring artifact and beam hardening corrections were applied, but only minimal smoothing was applied. Reconstructed images were further manipulated for viewing using two additional software packages. Fiji [12], a realization of the image analysis package ImageJ, was used to stack and crop regions of interest. OsiriX [13] was used for three- dimensional (mean or maximum) intensity projections and volume renderings. Rendered surfaces were made transparent to reveal the internal structures. In order to image and study larger volumes, two overlapping scans were merged using the 3D stitching routine [12]. The linear blending option was utilized.

X-ray tomography was performed on FS welded samples both with and without Ni foil present. In the no nickel foil sample tomography case, the imaged volume was

approximately 7 x 6.35 x 2.8 mm. Two linked voids were seen on the surface and the voids continued through the sample. Tool striations on the top surface were also evident. Figure 3 presents a three dimensional mean intensity projection of the nickel foil CP Ti FS weld. The imaged volume is approximately 13.86 x 6.35 x 2.8 mm. The nickel foil has been deformed, broken into flakes, and distributed by the FS process. A large piece of the original foil is present at the bottom of the weld. It is assumed that the foil is bent to the retreating side upon its initial contact with the rotating tool.

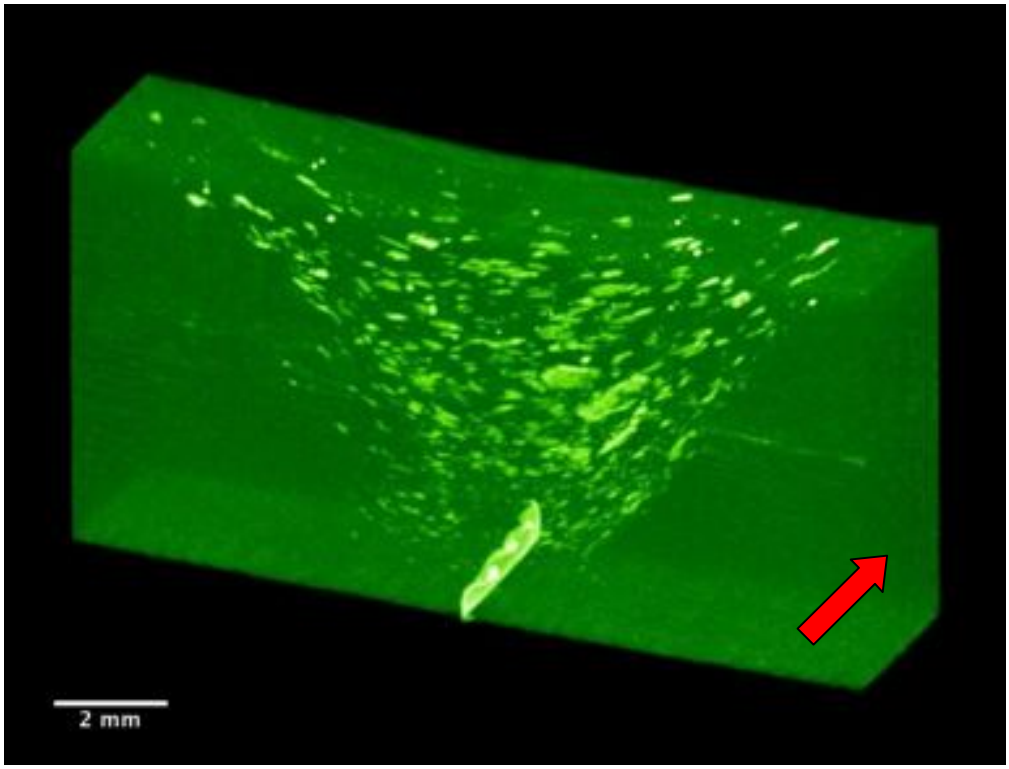

Figure 3 – A 3D mean intensity projection of a CP Ti FS weld with Ni marker foil (bright areas). Weld direction is indicated by the arrow.

Figure 4 presents sagital maximum intensity projections after subdividing the volume into the advancing and retreating subregions on either side of the weld mid-line, as marked by the remnant foil at the bottom of the weld. A 3D object counter [12, 14] measures 539 objects on the retreating side as opposed to 299 objects on the advancing side. The absolute number depends on the threshold gray scale selected but the relative ratio is fairly constant. Therefore, flake remnants are distributed asymmetrically in a ratio about 2/3 vs. 1/3. The advancing side (Fig. 4b) may be divided into four sub-regions based on the flake density, morphology, and alignment: these are the top, upper middle, lower middle, and bottom regions. The top region contains few flakes and those present appear randomly oriented. This region is likely to be heavily influenced by the tool shoulder. The upper middle region contains aligned flakes at angles of approximately 30-39 degrees down from the horizontal plane. The lower middle region also contains many aligned flakes but at higher angles; 46-56 degrees down from the horizontal. The bottom region contains many small, more random flakes. Some corresponding layering appears to be present in the retreating side, but this diminishes as the distance from the centerline increases. Some of the thinnest flakes observable in the tomograph measure approximately 50 μm, indicating a thickness reduction from the starting foil of a factor of two due to deformation.

If one divides the tomographic dataset into the four subregions identified in Figure 4, in effect creating four subsets, a maximum intensity projection in the perpendicular (bottom to top) direction can be formed of each one. These are shown in Figure 5. Note these regions are not of similar thickness and the remnant foil was eliminated from the bottom subregion for clarity. Note the low density and the relatively large sizes of flakes in the top subregion, the advancing-retreating side asymmetry (by 300-400 μm) in the middle subregions, and the symmetric, small homogenous flake distribution in the bottom subregion. The 3D object counter measures a plurality of the objects (≈43%) residing in the lower middle region (Fig. 5c) with the remaining objects roughly equally distributed in the remaining three regions. Also apparent is that the weld geometry was changing with tool travel, as the width of the marker distribution is generally wider at the top than at the bottom of each image (except for the bottom subregion). Small, spheroidal, bright (dense) particles may be seen in the upper two images and are believed to be tool wear debris. Little or no debris is seen in the bottom two subregions.

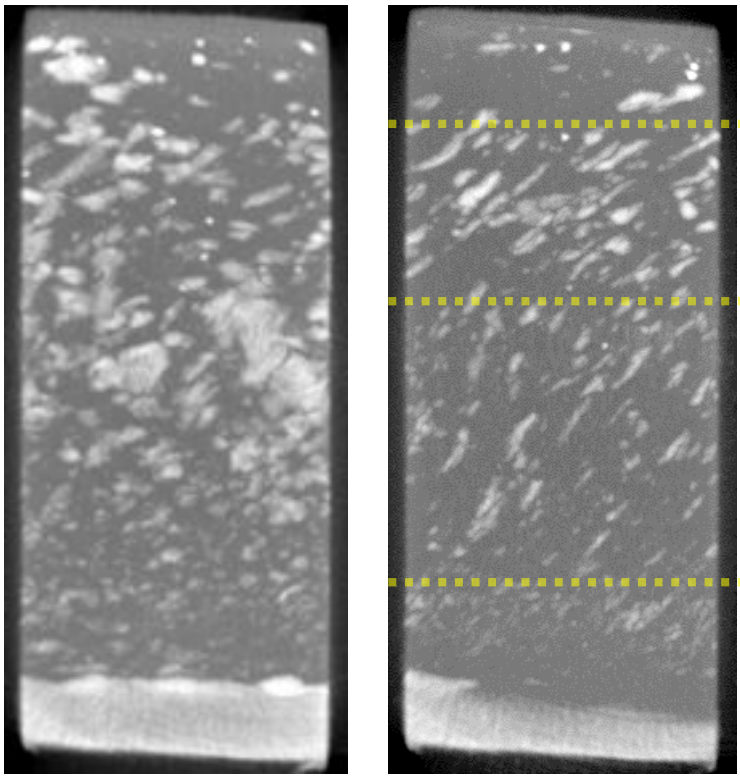

(a) (b)

Figure 4 – Maximum intensity projections of the (a) retreating and (b) advancing sides. The advancing side may be divided into four sub-regions based on the flake density, morphology, and alignment.

IV. Microstructural Characterization

Samples from the welded regions of both CP Ti and CP Ti with Ni were polished and prepared for SEM. Figure 6 present two images of nickel flakes and the surrounding regions. It is clear that the flake has been deformed and some material has diffused into the neighboring titanium. EDS confirms the presence of nickel in the matrix at the level of 2-7 atomic percent depending on phase. It is hypothesized that while at elevated temperature, the nickel diffuses into the CP Ti matrix, lowering the beta transus, and locally converting to the observed two phase microstructure upon cooling.

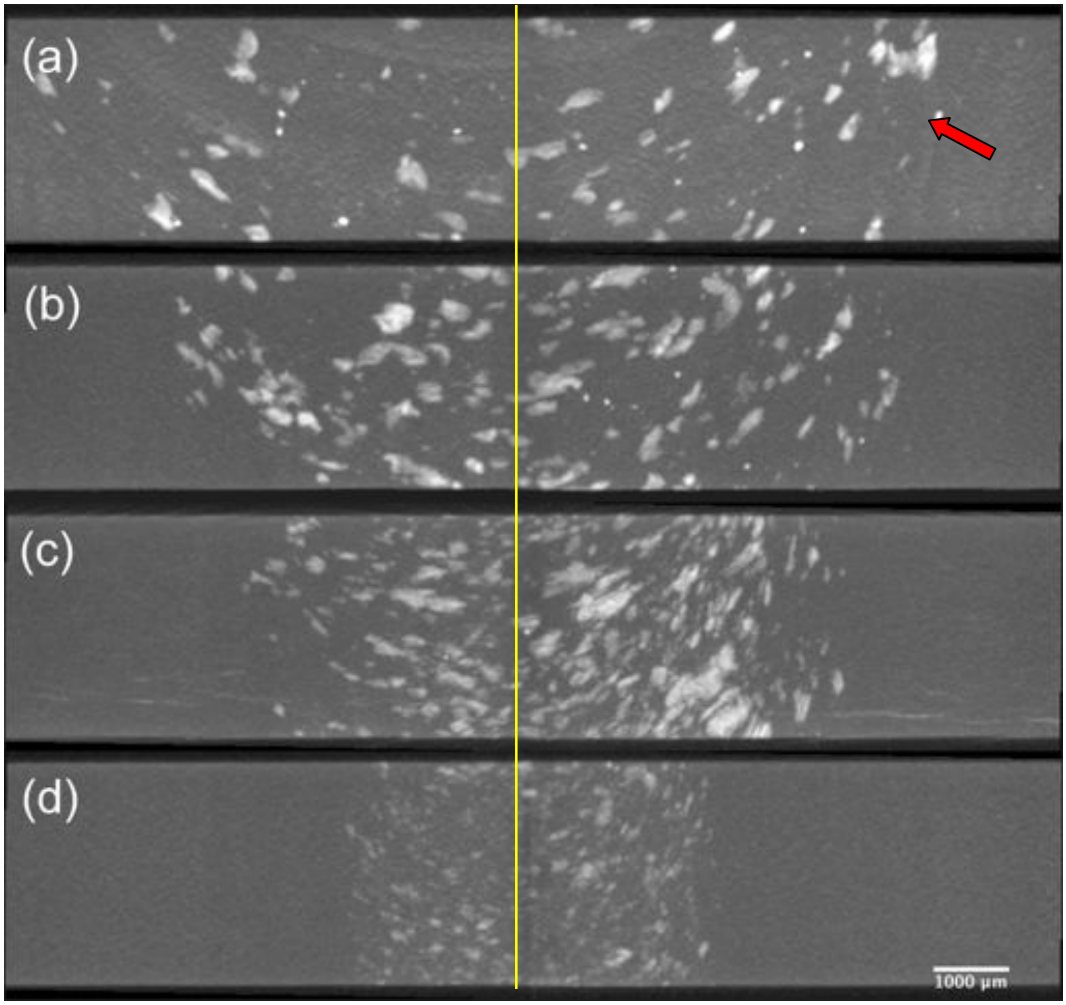

Figure 5 – Maximum intensity projections (a) top, (b) upper middle, (c) lower middle, and (d) bottom. The approximate original joint line is marked and the arrow points to possible tool debris. Advancing side is to the left while the weld direction is upwards towards the top of the page.

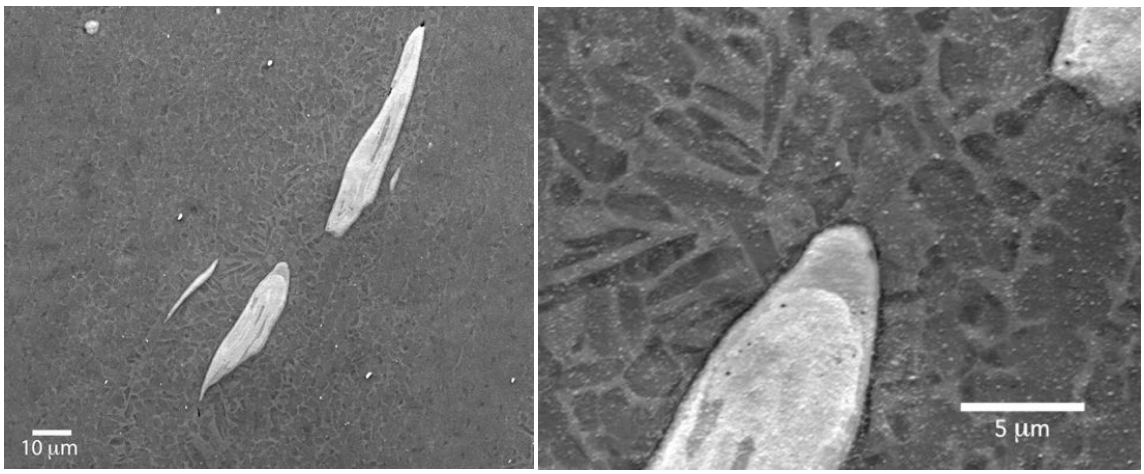

Figure 6 – SEM images of a Ni flake (left) and the microstructure of the titanium matrix surrounding the flake (right).

V. Mechanical Testing

Microsamples were prepared for local mechanical property testing to assess the effects of the nickel in the stir zone. Slices approximately 1 mm thick were cut using EDM from the weld zone of a plate made with similar welding parameters but a 300 mm long weld using a 0.1 mm Ni foil (sample labeled SD5 in this study). These slices were polished to thin and flatten the sample, and determine the location of the stir zone. Dog-bone-shaped microsamples, Figure 7, were then cut out of the slice using a positive-shaped graphite tool and a sinking EDM. These microsamples are nominaly about 3 mm long by 1 mm wide in size and have a gage section approximately 0.300 mm by 0.250 mm. Figure 7 (upper right) shows the locations of the microsamples, both within the stir zone and in the transition regions, before removal from the slice.

Probing the mechanical properties of the microsample requires an apparatus that is sensitive at the sub-micron scale. A system capable of mechanical testing at the sub-micron scale, called the μ-Material Testing System (μ-MTS) has been developed at UMBC. The μ-MTS is similar to the larger brethren MTS, except the need for isolating environmental vibrations, increased sensitivity of load, displacement, and strain, and stiction issues. In Figure 8, on the left side, is a picture of the μ-MTS apparatus with its key components labeled. The system consists of a piezo-actuator acting as the load train with a linear airbearing to reduce friction and stiction of the loading grip. Interchangeable load cells allow one to tailor the capacity of the load cell to have an optimized sensitivity. The use of microsamples does not allow the use of traditional strain gages or extensometers because of the sensitivity and physical barriers of the microsample size. Therefore, a non-contact strain measurement system is optimal. The system used in these experiments is an Interferometric Strain/Displacement Gage (ISDG) capable of measuring a 280 μm gage with ± 3.7 με uncertainty [15,16].

The microsamples exhibited a ductile behavior during testing. Figure 7 (lower right) shows an example of a failed specimen. Yield strengths for the stir zone were measured to be 463 and 459 MPa while the ultimate tensile strengths were 613 and 620 MPa for the upper and lower specimens, respectively. This compares favorably to the typical properties of CP Ti Grade 2 with yields of 335-545 MPa and UTSs of 510-605 MPa [17]. In the transition region, the measured yields varied from 306 MPa to 422 MPa with the average of six samples being 373 MPa. UTS varied from 458 MPa to 500 MPa with the average of six samples being 480 MPa. This is still comfortably above the minimum specified minimum yield of 275 MPa and UTS of 345 MPa. In other microsamples, with thinner Ni foils, yield strengths averaging 379 MPa and strains to failure as high as 25% have been measured.

VI. Discussion

The goal of this project was to use a nickel marker foil to help identify material flow in CP Ti friction stir welds. While the nickel foil has accomplished this, it must also be recognized that it significantly alters the FS conditions. Major differences include the weld loads, surface finish, and the presence of voids. These differences are potentially due to differences in metallurgical, tribological, or thermal conductivity properties. Future investigations will address these interactions more closely.

Markers record the final position of the material as it is deformed, distributed and deposited after the passing of the tool. The markers clearly show differences in material deposited in the advancing and retreating sides, and are capable of delineating different flows at different depths. Unlike previous aluminum FSW marker work [8], where the marker was offset to the advancing side and most marker material was deposited on the advancing side, here most marker materials were deposited on the retreating side.

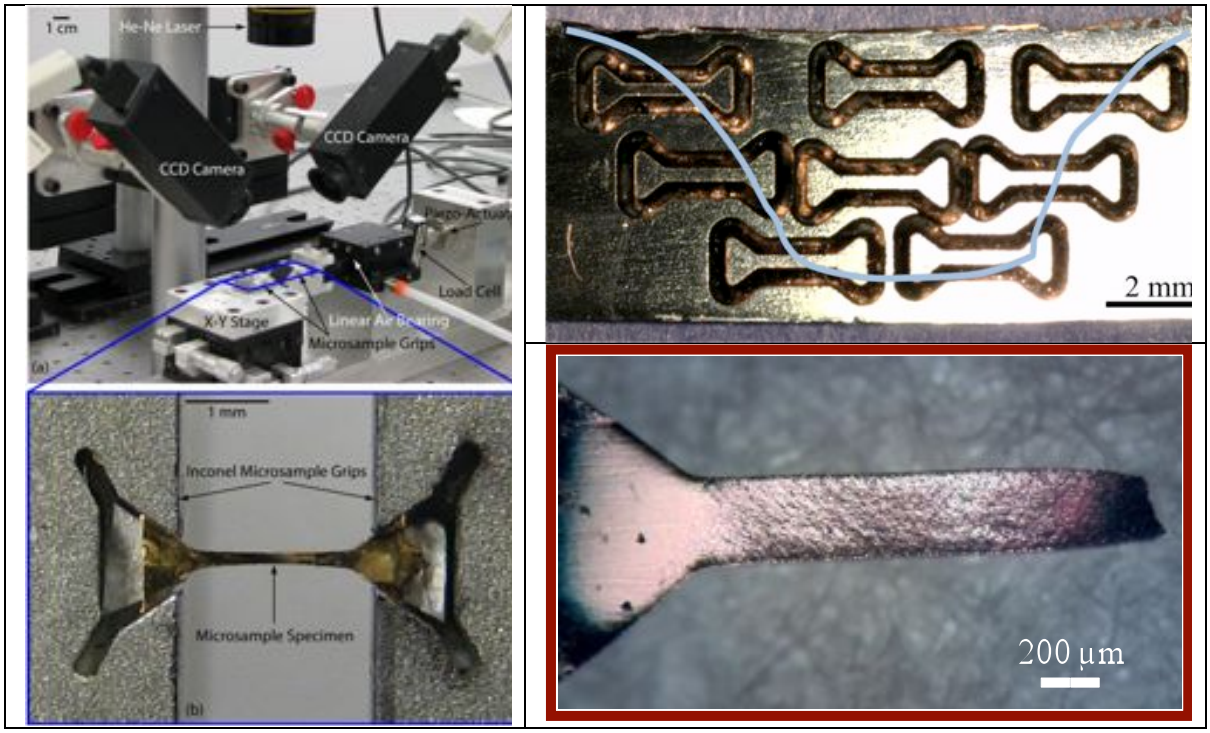

Figure 7 – A picture of the µ-Material Testing System (µ-MTS) apparatus and microsample in position in the grisp (left). Positions of samples taken from a CP Ti FSW with 0.004 inch thick Ni foil marker inserted (upper right). An example of a deformed and failed CP Ti microsample from the stir zone (lower right).

With the relatively few flakes present and the large amount of tool debris the top region is likely highly influenced by the tool shoulder. The bottom region with numerous, well-distributed small flakes may reflect flakes which have been ground down to smaller dimensions due to multiple passes around the tool or which may be too small to be pulled upwards by other flowing material. The two upper and lower middle regions are characterized by the alignment of the flakes. We hypothesize that the boundary between the two marks the distance that frictional heat (generated by the tool shoulder at the surface) can penetrate into the plate. Thus, the upper middle region is believed to be significantly warmer than the lower middle region.

It should be possible using the markers to define the maximal extent of the stir region, that is where the material velocity is zero, and thus aid computational modeling by providing experimental constraints to the possible solutions. Streamlines from computational models "indicate that beyond the region of recirculating plastic flow, i.e. in the transition zone, material transfer occurs mainly on the retreating side [18]."

In the future, we hope to perform more experiments with various thicknesses of marker foils, with the marker foil off the mid-plane, and with it perpendicular to the travel direction. These types of experiments may contribute to inferring the effects of tool design and FS processing parameters from the marker material distribution. Mechanical property measurements are planned.

Summary

X-ray tomography has been performed on CP titanium friction stir welds prepared with and without a nickel foil marker present. The marker foil welded sample had better surface finish

and no voids were visible in the weld, in contrast to the no foil sample which had voids. The tomography revealed the distribution of the deformed nickel. 3D image analysis was used to count objects on the advancing and retreating sides and maximum intensity projections show changes in the alignment of nickel flakes with depth in the weld.

Acknowledgements – The authors gratefully acknowledge funding from the Office of Naval Research, and the Basic Research Program of the Naval Research Laboratory. We furthermore acknowledge the assistance of Drs. Jerry Feng and Christian Widener.

References

[1] R.S. Mishra and M.W. Mahoney. Friction Stir Welding and Processing. *ASM (2007).*

[2] W.B. Lee, C.Y. Lee, W.S. Chang, Y.M. Yeon, S.B. Jung. "Microstructural investigation of friction stir welded pure titanium." *Materials Letters 59 (2005) 3315-3318.*

[3] O. Lorrain, V. Favier, H. Zahrouni, and D. Lawrjaniec, "Understanding the material flow path of friction stir welding process using unthreaded tools," *J. Materials Processing. Tech*nology, 210 (2010), pp. 603-609.

[4] S. Mukherjee, A.K. Ghosh, Flow Visualization and Estimation of Strain and Strain-Rate during Friction Stir Process, *Materials Science & Engineering A*, A527 (2010), pp. 5130-5135, doi:10.1016/j.msea.2010.04.091.

[5] R. K. Everett, K. E. Simmonds, A. Geltmacher, "Spatial Distribution of Voids In HY100 Steel by X-ray Tomography," *Scripta Materialia,* Vol. 44:(1), pp. 165-169, Jan, 19, 2001.

[6] J.P. Bandstra , D.A. Koss, A. Geltmacher, P. Matic, R.K. Everett, "Modeling void coalescence during ductile fracture of a steel," *Materials Science and Engineering*, A366 (Feb. 15, 2004), pp. 269–281.

[7] J. Wolk, R. K. Everett, and L. Salamanca-Riba, "Computed Tomography of Titanium Friction Stir Welds", in *EPD Congress 2010: Characterization of Minerals, Metals and Materials*, Proceedings of the TMS 2010 Annual Meeting & Exhibition, February 14-18, 2010, Washington State Convention Center , Seattle, WA.

[8] H.N.B. Schmidt, T.L. Dickerson, and J.H. Hattel, "Material flow in butt friction stir welds in AA2024-T3," *Acta Materialia* 54 (2006) 1199–1209.

[9] J. Schneider, R. Beshears, A. C. Nunes, "Interfacial sticking and slipping in the friction stir welding process," Materials Science and Engineering A 435–436 (2006) 297–304.

[10] H. Fujii, Y. Sun, H. Kato, and K. Nakata, "Investigation of welding parameter dependent microstructure and mechanical properties in friction stir welded pure Ti joints," *Materials Science and Engineering* A527 (2010) 3386–3391.

[11] http://www.skyscan.be/products/downloads.htm

[12] http://pacific.mpi-cbg.de/wiki/index.php/Main_Page

[13] http://www.osirix-viewer.com/

[14] S. Bolte & F. P. Cordelières, A guided tour into subcellular colocalization analysis in light microscopy, Journal of Microscopy, Volume 224, Issue 3: 213-232.

[15] W. N. Sharpe, *A potential optical standard for resistance strain gages.* Journal of Testing and Evaluation, (1998) 26(5): 481-488.

[16] M. Zupan and K.J. Hemker, "Application of Fourier analysis to the laser based interferometric strain/displacement gage*," Experimental Mechanics*, (2002) 42(2): 214-220.

[17] http://cartech.ides.com/

[18] R. Nandan, T. DebRoy, H.K.D.H. Bhadeshia, "Recent advances in friction-stir welding – Process, weldment structure and properties," *Progress in Materials Science* 53 (2008) 980–1023.